



UNIVERSITÀ POLITECNICA DELLE MARCHE  
Repository ISTITUZIONALE

Carboxymethyl cellulose-based hydrogel film combined with berberine as an innovative tool for chronic wound management

This is the peer reviewed version of the following article:

*Original*

Carboxymethyl cellulose-based hydrogel film combined with berberine as an innovative tool for chronic wound management / Cometa, S.; Licini, C.; Bonifacio, M. A.; Mastroilli, P.; Mattioli-Belmonte, M.; De Giglio, E.. - In: CARBOHYDRATE POLYMERS. - ISSN 0144-8617. - STAMPA. - 283:(2022). [10.1016/j.carbpol.2022.119145]

*Availability:*

This version is available at: 11566/295650 since: 2024-04-06T08:05:21Z

*Publisher:*

*Published*

DOI:10.1016/j.carbpol.2022.119145

*Terms of use:*

The terms and conditions for the reuse of this version of the manuscript are specified in the publishing policy. The use of copyrighted works requires the consent of the rights' holder (author or publisher). Works made available under a Creative Commons license or a Publisher's custom-made license can be used according to the terms and conditions contained therein. See editor's website for further information and terms and conditions.

This item was downloaded from IRIS Università Politecnica delle Marche (<https://iris.univpm.it>). When citing, please refer to the published version.

(Article begins on next page)

# **Carboxymethyl cellulose-based hydrogel film combined with berberine as an innovative tool for chronic wound management**

S. Cometa<sup>1#</sup>, C. Licini<sup>2#</sup>, M.A. Bonifacio<sup>3,4</sup>, P. Mastroiilli<sup>5</sup>, M. Mattioli-Belmonte<sup>2</sup>, E. De Giglio<sup>3,4\*</sup>

<sup>1</sup> Jaber Innovation S.r.l., Via Calcutta 8, 00144 Rome, Italy

<sup>3</sup> Department of Clinical and Molecular Sciences, Università Politecnica delle Marche, Via Tronto 10/a, 60126 Ancona, Italy

<sup>3</sup> Department of Chemistry, University of Bari, Via Orabona 4, 70126 Bari, Italy

<sup>4</sup> INSTM, National Consortium of Materials Science and Technology, Via G. Giusti 9, 50121 Florence, Italy

<sup>5</sup> DICATECh Department Politecnico di Bari, Via Orabona 4, 70126 Bari, Italy

# These authors equally contributed to the work

## **Corresponding author:**

\*Elvira De Giglio

Department of Chemistry, University of Bari “Aldo Moro”, via E. Orabona 4, Bari, 70126, Italy

elvira.degiglio@uniba.it

Tel./Fax: +39 0805442021

Mail of co-authors:

stefania.cometa@jaber.it (Cometa S.), c.licini@pm.univpm.it (Licini C.), maria.bonifacio@uniba.it

(Bonifacio M.A.), p.mastroiilli@poliba.it (Mastroiilli P.), m.mattioli@univpm.it (Mattioli-

Belmonte M.), elvira.degiglio@uniba.it (De Giglio E.),

**Keywords:** CMC-based film; berberine; keratinocytes; fibroblasts; topical delivery; chronic wound

### **Chemical compounds studied in this article**

Berberine Hydrochloride (PubChem CID: 12456); carboxymethyl cellulose sodium salt (PubChem CID: 6328154); hydroxyethyl cellulose (PubChem CID: 4327536) Acetylated distarch phosphate (PubChem SID: 24832109); bentonite clay (PubChem CID: 72941614); gallium nitrate (PubChem CID: 61635); boric acid (PubChem CID: 7628); 2,2-diphenyl-1-picrylhydrazylhydrate (DPPH) (PubChem CID: 2735032) ; 2,2'- azino-bis(ethylbenzotiazolinone-6-sulfonic) acid (ABTS) (PubChem CID: 5815211); lysozyme (PubChem CID 16130991).

### **Abstract**

Polysaccharide-based hydrogels are achieving remarkable performances in chronic wounds treatment. In this work, a carboxymethyl cellulose-based hydrogel film was developed to support skin repair. The hydrogel was loaded with berberine, a polyphenolic molecule endowing antioxidant and cytoprotective features. The film was physico-chemically characterized and *in vitro* tested on keratinocytes and fibroblasts subjected to oxidative stress. The biocomposite showed high thermal stability (onset decomposition temperature 245°C) and significant fluid uptake performances, both in free conditions (up to 6510%) and under external pressure (up to 3400%). Moreover, it was able to control oxidative stress and inflammation markers involved in wound chronicity. Keratinocytes hyperproliferation, features that normally hamper injury restoration, was reduced of 25%. Our results showed that the combination of berberine and hydrogel provides a synergic improvement of the material properties. The biocomposite represents a promising candidate for dermatological applications against oxidative stress at the chronic wound site, promoting the healing process.

## 1. Introduction

Skin is one of the most important defences that an organism uses to protect itself from environmental damages, such as bacteria and dehydration. When injuries occur, the skin barrier is interrupted, and the wound healing process starts, repairing the damaged tissue and re-establishing skin protection. This intricate process, involving immune and skin cells, consists in four subsequent stages: haemostasis, inflammation, proliferation, and remodelling (Zhao et al., 2016; Morton et al., 2016). Inflammation is crucial in wound healing, as in this step neutrophils secrete cytokines and growth factors to recruit other immune cells (*i.e.*, macrophages), which will have critical effects in the next re-epithelialization, matrix synthesis, and angiogenesis (Zhao et al., 2016; Tejiram et al., 2016). When the inflammatory stage enters a self-renewing state and the system fails to proceed through the normal orderly sequence, the wound becomes chronic (Zhao et al., 2016).

An ideal wound dressing material should support skin regeneration processes without interfering with the timing and coordination of cells and growth factors activities (Stan et al., 2021). Since fibrotic tissue takes place when skin repair mechanisms become abnormal, sustained by oxidative stress and persistent inflammation (Condorelli et al., 2021), chronic wounds require proper dressings to speed up healing processes, shifting the clinical goal from skin repair to regeneration (Jiang & Rinkevich, 2021).

Hydrogels, hydrocolloid films, and foams could be successfully exploited to develop smart wound dressings, being active materials able to restore skin functions while reducing aesthetic impact (Bal- Öztürk et al., 2021). Hydrogels are particularly suitable materials for a wound-healing treatment, thanks to their moisturizing and biocompatible features (Asadi et al., 2020) as well as intriguing mechanical properties (Zhang M. et al., 2021). In addition, polysaccharide-based hydrogels combine these features with environmental sustainability and degradability (Hu & Xu, 2020). In particular, carboxymethyl cellulose (CMC) based materials showed outstanding wound

healing characteristics (Kanikireddy et al., 2020). Moreover, blends of CMC with other polysaccharides were recently used as bioinks for artificial skin fabrication (Zhang K. et al., 2021). Starting from an innovative class of eco-friendly, cytocompatible CMC-based hydrogels with tuneable skin delivery properties (Cometa et al., 2021), this work focuses on the development of an innovative berberine-loaded hydrogel formulation for the healing of chronic wounds. Even if berberine's antioxidant properties and its potential role in wound healing have already been shown (Cometa et al., 2021; Zhang et al., 2020), the combined effect of berberine and carboxymethyl cellulose has not been investigated yet. Preliminary studies (Cometa et al., 2021) described four different CMC-based hydrogel films preparation procedures, as well as the swelling kinetics and the *in vitro* skin permeation performances of the relevant berberine loaded films. The berberine release kinetics from the CMC-based films, investigated by Franz cell, allowed us to choose, among the four films developed, the most promising candidate for wound healing applications.

In this study, a detailed physico-chemical characterization of this CMC-based hydrogel film, by spectroscopic (FT-IR/ATR, XPS, Solid-state NMR and SEM), thermogravimetric, *in vitro* antioxidant activity assessment and enzymatic biodegradation by lysozyme is reported, highlighting the role of the carbohydrate in the biocomposite formulation and its interaction with the bioactive molecule. Liquid uptake studies, in different conditions (i.e., carried out both in free conditions and under an external pressure), evidenced the swelling capability of the carbohydrate-based film, also when loaded with berberine.

Moreover, the wound healing capabilities were investigated, evaluating the potential effect of these customized hydrogels on keratinocytes and fibroblasts, paying particular attention to their antioxidant and anti-inflammatory activities and their role on re-epithelialization and extracellular matrix formation. We hypothesized that the inclusion of berberine in a CMC-based hydrogel could enhance the material wound healing properties also providing antioxidant features. The developed material represents a smart dressing for chronic wound treatment.

## 2. Materials and Methods

### 2.1 Materials


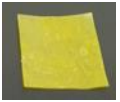
Carboxymethyl cellulose sodium salt, CMCNa (MW 700 kDa, DS 0.7, pharmaceutical grade) and hydroxyethyl cellulose, HEC (MW 250 kDa MS 2, viscosity 80–125 cm/s, food grade) were purchased from Eigenmann e Veronelli S.p.A. (Milan, Italy). Bentonite (BENT) was supplied by Dal Cin S.p.A. Sesto San Giovanni (Milan, Italy) and Laponite<sup>®</sup> RD was supplied by Byk (Altana Group, Wesel, Germany). Acetylated distarch phosphate (ADP) was supplied by Romana Chimici S.p.A. (Palo del Colle, Bari, Italy). Berberine hydrochloride from *Berberis aristata* dry extract at 98% (BERB) was purchased from Farmalabor s.r.l. (Canosa di Puglia, Apulia, Italy). Gallium nitrate ( $\text{Ga}(\text{NO}_3)_3$ ) and ethanol, as well as ultrapure water and methanol (all HPLC grade), were purchased from Sigma Aldrich (Milan, Italy).

### 2.2 Hydrogel film preparation and BERB loading procedure

Hydrogel films were prepared exploiting a procedure optimized in a previous work (Cometa et al., 2021) and described in the following. Briefly, CMCNa, HEC and ADP polymers, in the ratio 3:1:0.12 w/w, were mixed to bentonite and Laponite<sup>®</sup> powders (in the ratio 10:1, w/w). In this mixture, the clays were 10% w/w of the content of the polymers. The mixture was dispersed in distilled water (in the range 2% w/v) containing  $\text{Ga}(\text{NO}_3)_3$  at 2% w/w respect to the content of the polymers, until the complete homogenization and hydration of polymers and clays mixture is achieved. The smooth and homogeneous film-forming solution was transferred in an ultrasonication bath to remove air bubbles and then cast on Petri dishes (diameter 17 cm) and dried at 80°C for 3 hours. Successively, the films underwent a second crosslinking procedure, employing a surface crosslinking solution containing  $\text{Ga}(\text{NO}_3)_3$  at 10% w/w respect to the film weight. The solution was sprayed over both the surfaces of the film and the latter was successively dried at 80°C for 1 hour (film coded as HG<sub>sx</sub>). To obtain BERB-loaded films, BERB was dissolved in a part of the distilled water employed in the hydrogel film preparation (film coded as HG<sub>sx</sub>-BERB).

The obtained hydrogel films compositions were reported in Table 1.

**Table 1.** Hydrogel films composition

Film	Percentage of each component to the total mass of dried film (%)							
	CMCNa	HEC	ADP	BENT	LAP	BERB	Bulk crosslinker	Surface crosslinker
HG <sub>sx</sub> 	58.7	19.6	2.3	7.8	0.8	--	1.6	9.1
HG <sub>sx</sub> -BERB 	53.5	17.8	2.1	7.1	0.7	8.1	1.5	9.1

### 2.3 Chemical, physical and thermal characterization

Hydrogel films were characterized by Fourier-Transform Infrared Spectroscopy (FT-IR) in Attenuated Total Reflectance mode (ATR), Thermo-Gravimetric Analysis (TGA), swelling performances tests, X-ray Photoelectron Spectroscopy (XPS), Solid-state Nuclear Magnetic Resonance (SS NMR). Moreover, morphological investigations, by means of Scanning Electron Microscopy (SEM), have been reported in the Supplementary Material.

Dry samples, without pretreatment, underwent FT-IR (ATR) analyses through a Spectrum Two PE instrument supplied by PerkinElmer, endowed with a universal ATR accessory (UATR, Single Reflection Diamond/ZnSe). For each of the relevant samples, FT-IR/ATR spectra were recorded from 400 to 4000cm<sup>-1</sup> with a 4cm<sup>-1</sup> resolution.

Furthermore, the pure berberine, as well as the hydrogel films, were examined by TGA analyses through a PerkinElmer TGA-400 instrument (PerkinElmer Inc.). Briefly, 5-10mg of samples were heated in air-saturated atmosphere in the range of 30-800°C, with a constant flow rate (20°C/min) and a gas flow set at 20mL/min. The TGA Pyris series software was exploited to record thermograms (TG), calculate their respective derivative curves (DTG) and for further data mining.

Free swell capacity (FSC) was tested both in phosphate buffer solution (PBS, pH 7.4), using square-shaped samples (1cm x 1 cm) and placing them into sealed tea bags, using the method previously described (Cometa et al. 2021). The absorbency under load (AUL) was tested in PBS, when the sample (circle of 3 cm in diameter) is pressurized with a load of 0.3 psi, using the experimental setup reported by Zohuriaan-Mehr (Zohuriaan-Mehr et al., 2008). In both the tests, the water uptake was detected after 1 h.

The equations used for FSC(%) and AUL(%) are reported below:

$$\text{FSC(\%)} \text{ or } \text{AUL(\%)} = (W_s - W_d) / W_d \times 100\% \quad (1)$$

Where  $W_s$  and  $W_d$  represented the weight of the swollen and dry film, respectively.

XPS analyses were performed on a scanning microprobe PHI 5000 VersaProbe II, purchased from Physical Electronics (Chanhassen, MN). The instrument is equipped with a micro-focused monochromatized  $\text{AlK}\alpha$  X-ray radiation source. The hydrogel films, as well as bare BERB, were examined in HP mode with an X-ray take-off angle of  $45^\circ$  (instrument base pressure  $\sim 10^{-9}$  mbar.). The size of the scanned area was about  $1400 \times 200 \mu\text{m}$ . Wide scans and high-resolution spectra were recorded in FAT mode for each sample, setting pass energy values equal to 117.4eV and 29.35eV, respectively. In order to fit the high-resolution spectra, the commercial MultiPak software, version 9.9.0, was used. Atomic percentages were inferred from peak areas, previously normalized by MultiPak library's sensitivity factors. Adventitious carbon C1s was set as reference charge (284.8eV).

Solid-state NMR experiments were performed on a Bruker Avance I 400 spectrometer (operating at a frequency of 100.6 MHz for  $^{13}\text{C}$ ) using a 4.0 mm HX MAS probe at 298 K. For MAS experiments, samples were packed in zirconia rotors.  $^1\text{H}$ - $^{13}\text{C}$  CP/MAS NMR experiments were performed using 3.25  $\mu\text{s}$  proton  $\pi/2$  pulse length,  $\nu_{\text{CP}}$  of 55.0 kHz, contact time of 1.0 s,  $\nu_{\text{dec}}$  of 76.9 kHz and recycle delay of 2.0 s. A two-pulse phase-modulation (TPPM) decoupling scheme was used for the  $^1\text{H}$  decoupling. Chemical shifts for  $^{13}\text{C}$  were referenced to the methylene signal of adamantane ( $\delta$  38.48).



#### *2.4 Cell culture*

Human immortalized keratinocytes (HaCaT) and normal human dermal fibroblasts (NhDF) were cultured in High Glucose Dulbecco's Modified Eagle Medium (HG-DMEM; Corning Inc., Corning, NY, USA), supplemented with 10% foetal bovine serum (Corning Inc.), 1% L-glutamine (Thermo Fisher Scientific, Waltham, MA, USA) and 1% penicillin/streptomycin (Thermo Fisher Scientific), at 37 °C with 5% CO<sub>2</sub>. To simulate oxidative stress conditions, cells were treated with 200 mM H<sub>2</sub>O<sub>2</sub> for 24 h, then the medium with H<sub>2</sub>O<sub>2</sub> was replaced with basal medium, HGsx and HGsx-BERB conditioned medium, or medium containing 50 μM BERB as previously described (Cometa et al., 2021), to mimic the potential reparative effects of the films during the wound healing process.

#### *2.5 Cell viability*

To investigate cell viability,  $1.6 \times 10^4$  HaCaT cells/well and  $2.6 \times 10^3$  NhDF cells/well were seeded into 96-well plates and cultured as described above. Cell viability was evaluated by sodium 3'-[1-(phenylaminocarbonyl)-3,4-tetrazolium]-bis(4-methoxy-6-nitro)benzene sulfonic acid hydrate (XTT) colorimetric assay (Sigma-Aldrich) at 48 h, according to the manufacturer's instruction. Absorbance at 555 nm was read with 655 nm as reference wavelength using MultiskanGO plate reader (Thermo Fisher Scientific).

#### *2.6 Intracellular Reactive Oxygen Species (ROS) detection*

$2.5 \times 10^4$  cells/well were seeded in dark, clear-bottom 96-well plates and treated for 48 h. To evaluate intracellular ROS concentration, DCFDA/H<sub>2</sub>DCFDA Cellular ROS Assay Kit (Abcam) was used according to the manufacturer's instruction. ROS were detected by fluorescence microplate reader Infinite 200 PRO (Tecan, Männedorf, Switzerland) with excitation/emission at 485 nm/535 nm.

#### *2.7 Double-labelled and Ki67 immunofluorescence*

HaCaT and NhDF were seeded on 4-well chamber slides at a cell density of  $9 \times 10^4$  and  $1.4 \times 10^4$  cells/well, respectively, and treated as described above. After 48 h, cells were fixed with 4%

paraformaldehyde in PBS pH 7.4 (Santa Cruz Biotechnology, Dallas, TX, USA) at 4 °C for 30 min and washed in PBS, before permeabilization with 0.1% Triton X-100 in PBS at RT for 30 min. For double-labelling staining, HaCaT were incubated with anti-E-cadherin antibody (1:100, sc-8426, Santa Cruz Biotechnology) overnight at 4°C to evidence cell-cell junctions.

NhDF were instead incubated with anti-Fibronectin antibody (1:400, F6140, Sigma-Aldrich) overnight at 4 °C to underline cytoplasmic and extracellular protein expression. For Ki67 staining, HaCaT were incubated with anti-Ki67 antibody (1:100, sc-56319, Santa Cruz Biotechnology) overnight at 4 °C. Protocols are detailed in the Supplementary Material.

NIS-Elements microscope imaging software (Nikon, Milan, Italy) was used to capture images.

### *2.8 Wound healing assay*

HaCaT were seeded in a 12-well plate at a cell density of  $2 \times 10^5$  cells/well and treated as stated before. After they reached 100% confluence, cells were treated as mentioned above and a wound was performed in each well by a 1000 µl tip at time point 0. Images were taken at 6h and 24h after wound execution and the closing area percentage was analysed by Fiji software (Schindelin J. et al., 2012).

### *2.9 Western Blotting*

Cells ( $5 \times 10^5$  HaCaT/well and  $8 \times 10^4$  NhDF/well) were seeded in 6-well plates and treated as stated before. After 48 h, cells were detached by Trypsin 1X to collect pellets. For protein extraction, pellets were incubated for 30 min with RIPA buffer supplemented with 1 mM phenylmethylsulphonyl fluoride (PMSF), protease inhibitors (Sigma-Aldrich) and PhosStop (Roche) and centrifuged at 12000 g 10 min at 4 °C to collect the supernatant.

DC protein assay (Bio-Rad) was performed to measure the total protein amount and protein samples were prepared to load 20 µg of protein for each sample. Detailed protocol is described in the Supplementary Material. Acquisition was performed with Alliance Mini HD9 (Uvitec, Cambridge, UK) and densitometry was analysed with ImageJ software.

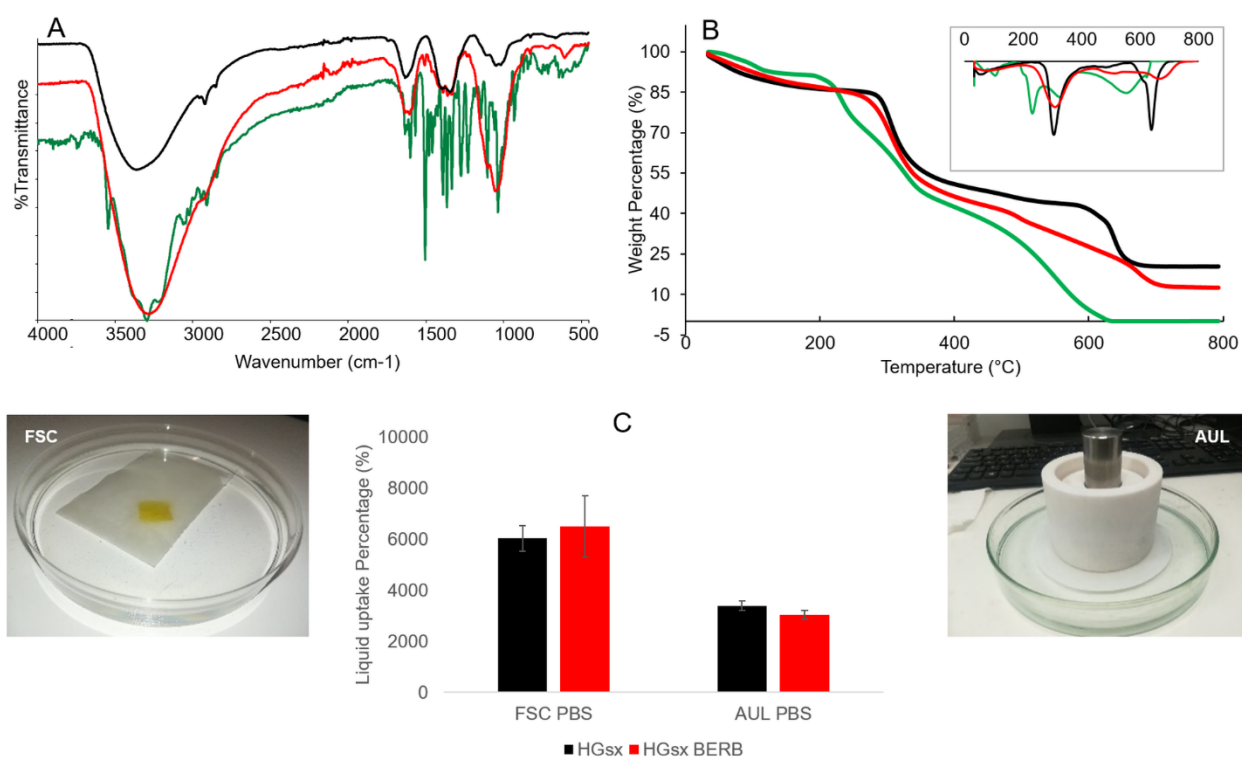
### *2.10 Statistical analysis*

The statistical analysis was performed using GraphPad Prism 7 (GraphPad Software, San Diego, CA). Cell viability results, as well as ROS detection and protein expression, were analysed by one-way ANOVA test. Wound healing results were analysed by two-way ANOVA test. After ANOVA, multiple comparisons among the groups were analysed by Tukey's test. Statistical significance was considered at  $p < 0.05$ .

### **3. Results and Discussion**

#### *3.1 Chemical, physical and thermal characterization of the prepared hydrogels*

Figure 1A shows the FTIR spectra of BERB, HGsx and HGsx-BERB hydrogel films. As far as BERB spectrum is concerned, it exhibited significant peaks at  $2920\text{ cm}^{-1}$  and  $2850\text{ cm}^{-1}$  that represent C–H stretching (alkanes),  $1505\text{ cm}^{-1}$  (aromatic C=C vibrations),  $1103\text{ cm}^{-1}$  (ring deformation and CH in-plane bending) and  $1035\text{ cm}^{-1}$  (C–H vibrations). In the case of the films, all the characteristic bands of CMC-based materials were present. The broad absorption bands at around  $3230\text{ cm}^{-1}$  are attributed to the -OH stretching, while at  $2880\text{ cm}^{-1}$  corresponds to the stretching of C-H in the cellulose structure (Kumar et al., 2020). The sharp absorption bands at  $1585$  and  $1410\text{ cm}^{-1}$  are due to the asymmetric and symmetric stretching of the  $\text{-COO}^-$  groups (Hebeish, Hashem, Abd El-Hady & Sharaf, 2013). In addition, the band at  $1320\text{ cm}^{-1}$  is due to the symmetrical deformations of  $\text{CH}_2$  attached to the carboxyl groups. The bands between  $1000$  and  $1200\text{ cm}^{-1}$  are attributed to the -C-O- stretching on the polysaccharide skeleton. A similar pattern was observed for the BERB-loaded film with evidence of the most intense polyphenol absorptions (i.e., the peak at  $1506\text{ cm}^{-1}$  and the shoulder at  $1103\text{ cm}^{-1}$ ).



**Fig. 1.** FT-IR/ATR spectra (A), TGA (B) and DTGA (in the inset) of HGsx film (black line), BERB (green line) and HGsx-BERB film (red line); free swell capacity and absorption under load (C) of HGsx and HGsx-BERB films after 1h in PBS.

TGA analysis of BERB, reported in Fig. 1(B) highlights a first thermal event related to the evaporation of water and/or volatiles up to 100°C (5.6%). Successively, three thermal events, at 199, 392 and 640°C, with weight losses of 22, 28 and 36%, respectively, are observed. The first one is relevant to the drug melting, the second to the BERB decomposition and the third one can be ascribed to the destruction of the BERB skeleton structure (Gao, Fan, Song, Zhang & Liu, 2020).

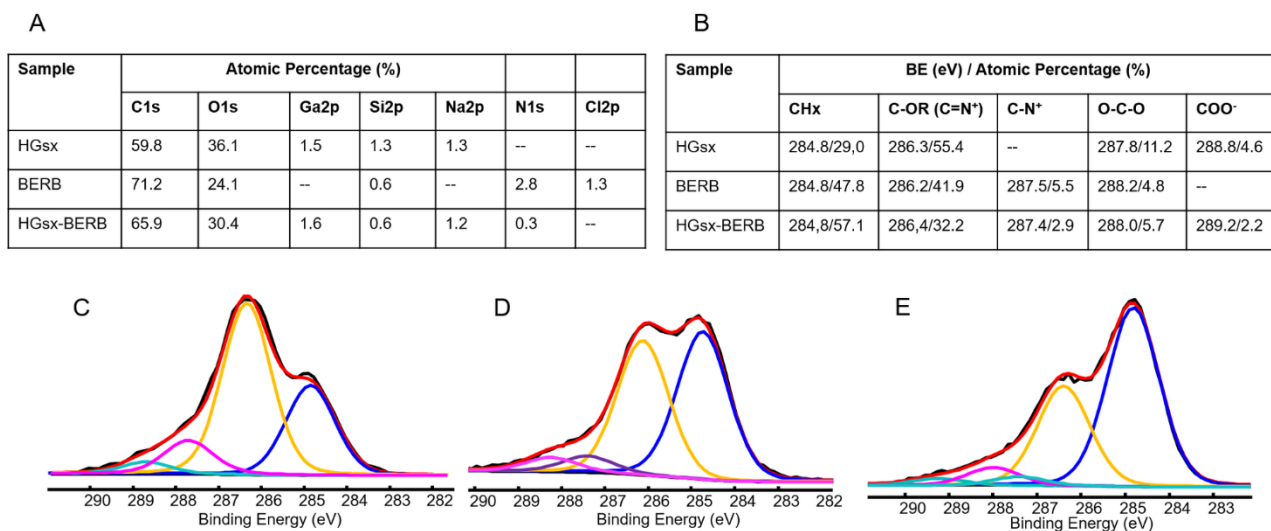
For polysaccharide-based hydrogels, even reported in Fig. 1(B), the first stage is related to water loss and it can be separated in two steps: removal of free water (below 110°C) and vaporization of bound water tightly attached to polymer matrix (below 240°C). The second stage can be ascribed to the decarboxylation of CMCNa with elimination of CO<sub>2</sub> (Lin et al., 2013) and decomposition of cellulosic materials. The third one to the decomposition of the other organic residues of CMCNa, HEC and modified starch, as well as to the other non-cellulosic materials present in the hydrogel composition (Oun & Rhim, 2015). It can be observed a slight anticipation of the second degradation

step (due to the overlapping of the BERB and polymer degradation steps), as well as a flattening of the third one for the hydrogel sample loaded with BERB, which can be ascribed to the presence of the active compound, as it can be better visualized by the DTGA reported in the inset of Fig. 1(B). It is noteworthy to mention that both HGsx and HGsx-BERB films resulted highly thermally stable, with an onset decomposition temperature falling at 278 and 246°C, respectively. The recorded residues at 800°C are 0, 20.3 and 12.6% for BERB, HGsx and HGsx-BERB samples, respectively. The decrease in the residue value for the BERB-loaded film is an indication of the presence of the active principle.

The developed hydrogels are polysaccharide based hydrophilic networks able to absorb and retain high liquid amounts. In a previous work (Cometa et al., 2021), the swelling kinetics up to 24 h in PBS were monitored both for the bare and for the BERB-loaded films. Here, we investigated the ability of the hydrogels to uptake aqueous fluids both in free conditions (FSC test) and when being submitted to mechanical action (compression), simulating a pressure exerted by a part of the body on the hydrogel film (AUL test). In Figure 1(C), the results, in terms of liquid uptake percentage, as well as in free and under load conditions, were reported for HGsx and HGsx-BERB samples. The requirement for a wound dressing device is that it must maintain its shape, remain soft, wet and able to absorb fluids, also under the stress of an external pressure. In this respect, considerable fluid uptake amounts in load-free conditions (ranging in 6040-6510%), were recorded, independently from the presence of BERB. These results allowed us to classify these materials as superabsorbent polymers, highlighting the fundamental role of the carbohydrate moieties. Indeed, swelling performances even superior to similar CMC-based materials proposed for wound dressing applications (Capanema et al., 2018) have been obtained. More interestingly, in the experimental setup carried out under pressure, high fluid amounts were still absorbed (in the range 3040-3400 g/g), evidencing an intriguing gel strength of our carbohydrate-based films also in their swollen state.

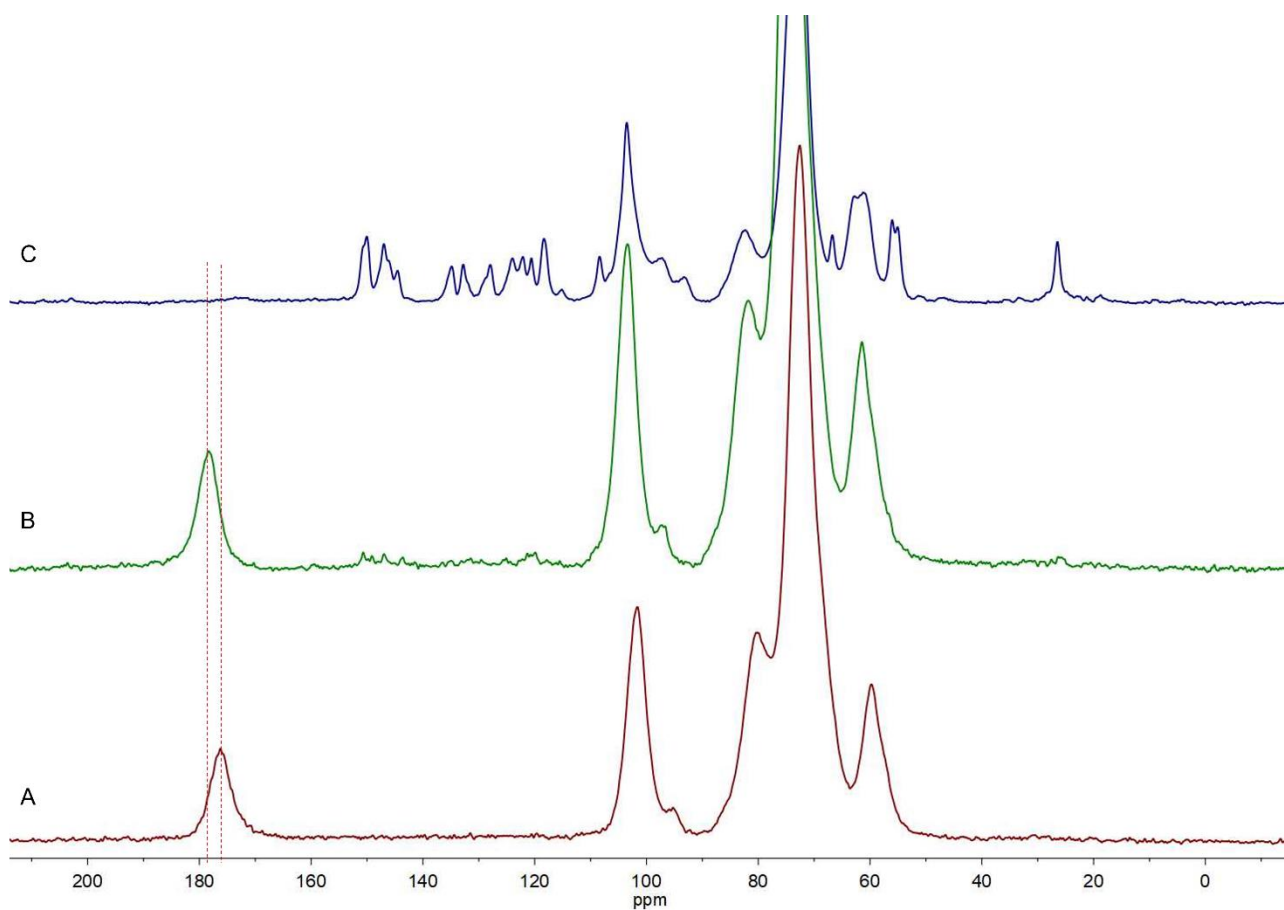
To obtain information on the surface composition and on possible interactions between the film and the active ingredient, XPS analysis was performed on both pure and BERB-loaded film, as well as on the pure polyphenolic extract. The elemental composition of all the samples is reported in Fig. 2(A); the loading of BERB within the film is confirmed by the presence of the N1s signal.

Additional information could be obtained by the C1s curve fittings, reported in Figs. 2(B-E). In the case of HGsx film, the C1s signal was fitted by four peaks: the first one, relevant to hydrocarbon contamination (CH<sub>x</sub>, fixed at 284.8 eV); the second one, typical of alcoholic or ether groups, predominant in carbohydrates (C-OH(R), 286.3eV); the third one, relevant to the hemiacetal group (O-C-O, 287.8eV); the last one, typical of carboxylate groups of the carboxymethyl moieties (COOH(R), 288.8eV). In the case of BERB, beyond the aliphatic and aromatic carbons (CH<sub>x</sub>, fixed at 284.8 eV), an important peak falling at 286.2eV is ascribable both to C-OR and C=N<sup>+</sup> present in the chemical formula of berberine (Trapani et al., 2011). Moreover, an additional peak falling at 287.5 eV is related to the C-N<sup>+</sup> moiety. Finally, the last peak is due to the O-C-O group, falling at 288.2eV. In the BERB-loaded film, all the peaks relevant both to the hydrogel and to BERB are evident. In addition, a +0.4 eV shift of the carboxylate groups was recorded. It could be hypothesized that an interaction between the COO<sup>-</sup> groups of the hydrogel and the N<sup>+</sup> of BERB occurred.

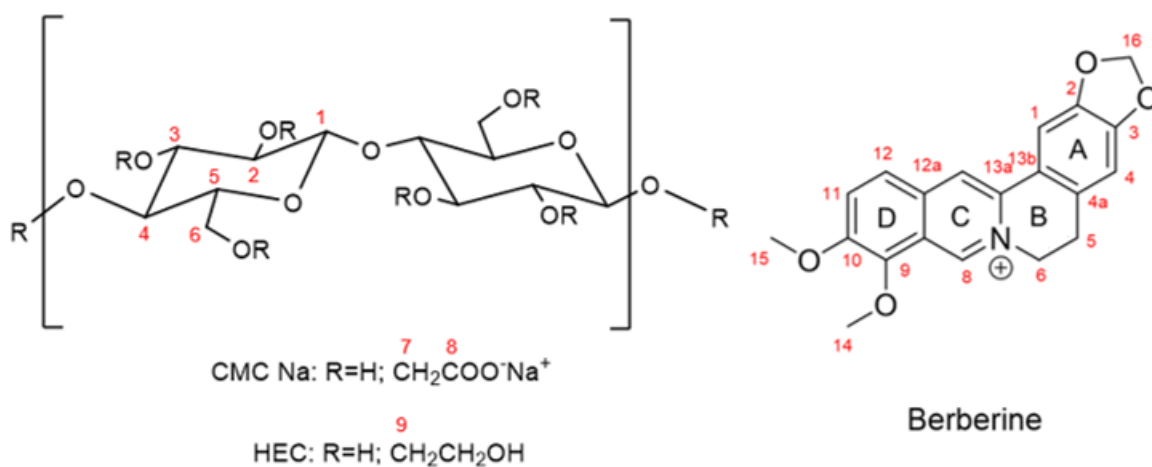


**Fig. 2.** XPS surface composition (A) and C1s curve fitting peaks attributions (B) relevant to HGsx (C), BERB (D) and HGsx-BERB (E). The maximum error on the binding energy values was equal to +0.2 eV.

Figure 3 shows the  $^1\text{H}$ - $^{13}\text{C}$  CP MAS spectra of HGsx, HGsx-BERB and commercial berberine. In the spectrum of HGsx, intense signals of carboxymethylcellulose are present at  $\delta$  176.2 (carboxylic  $\text{C}^8$ , see Scheme 1 for numbering),  $\delta$  101.7 ( $\text{C}^1$ ),  $\delta$  80.1 ( $\text{C}^4$ ),  $\delta$  72.5 ( $\text{C}^2$ ,  $\text{C}^3$ ,  $\text{C}^5$ ,  $\text{C}^7$ ) (this signal contains also a contribution by  $\text{C}^9$  of HEC, see Scheme 1 for numbering) and  $\delta$  59.5 ( $\text{C}^6$ ) (this signal contains also a contribution by  $\text{C}^{10}$  of HEC, see Scheme 1 for numbering). While the signal at  $\delta$  176.2 is specific for CMCNa, the remaining signals are also due to the carbons of HEC present in the film (Capitani et al., 2000). The  $^1\text{H}$ - $^{13}\text{C}$  CP MAS spectrum of HGsx-BERB shows signals of CMC/HEC at slightly different chemical shift, as a consequence of an interaction of the cellulosic materials with berberine. The highest difference in chemical shift was registered for the carboxyl carbon signal ( $\delta$  178.3), confirming the interaction between the  $\text{COO}^-$  groups of the hydrogel and the  $\text{N}^+$  of BERB, anticipated by XPS study. For HGsx-BERB, the chemical shifts of the anomeric carbons ( $\text{C}^1$ ), of  $\text{C}^4$ , and of  $\text{C}^6$  (cellulosic backbone) fell at  $\delta$  103.4,  $\delta$  81.8 and  $\delta$  61.4 while  $\text{C}^2$ ,  $\text{C}^3$ ,  $\text{C}^5$ ,  $\text{C}^7$  gave rise to a broad intense peak at  $\delta$  74.2. Weak signals due to berberine (Huang et al., 2005) are also visible in the spectrum of HGsx-BERB at  $\delta$  from 153 to 116 ppm (aromatic carbons) and at  $\delta$  25.9 ( $\text{C}^5$ , see Scheme 1). The  $^1\text{H}$ - $^{13}\text{C}$  CP MAS spectra of CMCNa and HEC are reported in the Supplementary Material.



**Fig. 3.**  $^1\text{H}$ - $^{13}\text{C}$  CP MAS spectra of HGsx (A), HGsx-BERB (B) and commercial berberine (C). T = 298 K, spin rate = 10 kHz for all experiments.



**Scheme 1.** Numbering used for  $^{13}\text{C}$  attributions of CMCNa, HEC and berberine.



SEM morphological investigations have been performed on both HGsx and HGsx-BERB. The obtained results have been shown in the Supplementary Material.

Moreover, *in vitro* antioxidant activity of BERB and HGsx-BERB by DPPH and ABTS assays as well as hydrogel enzymatic biodegradation by lysozyme have been reported in the Supplementary Material.

### *3.2 Evaluation of oxidative stress in keratinocytes and fibroblasts*

#### *3.2.1 Cell viability*

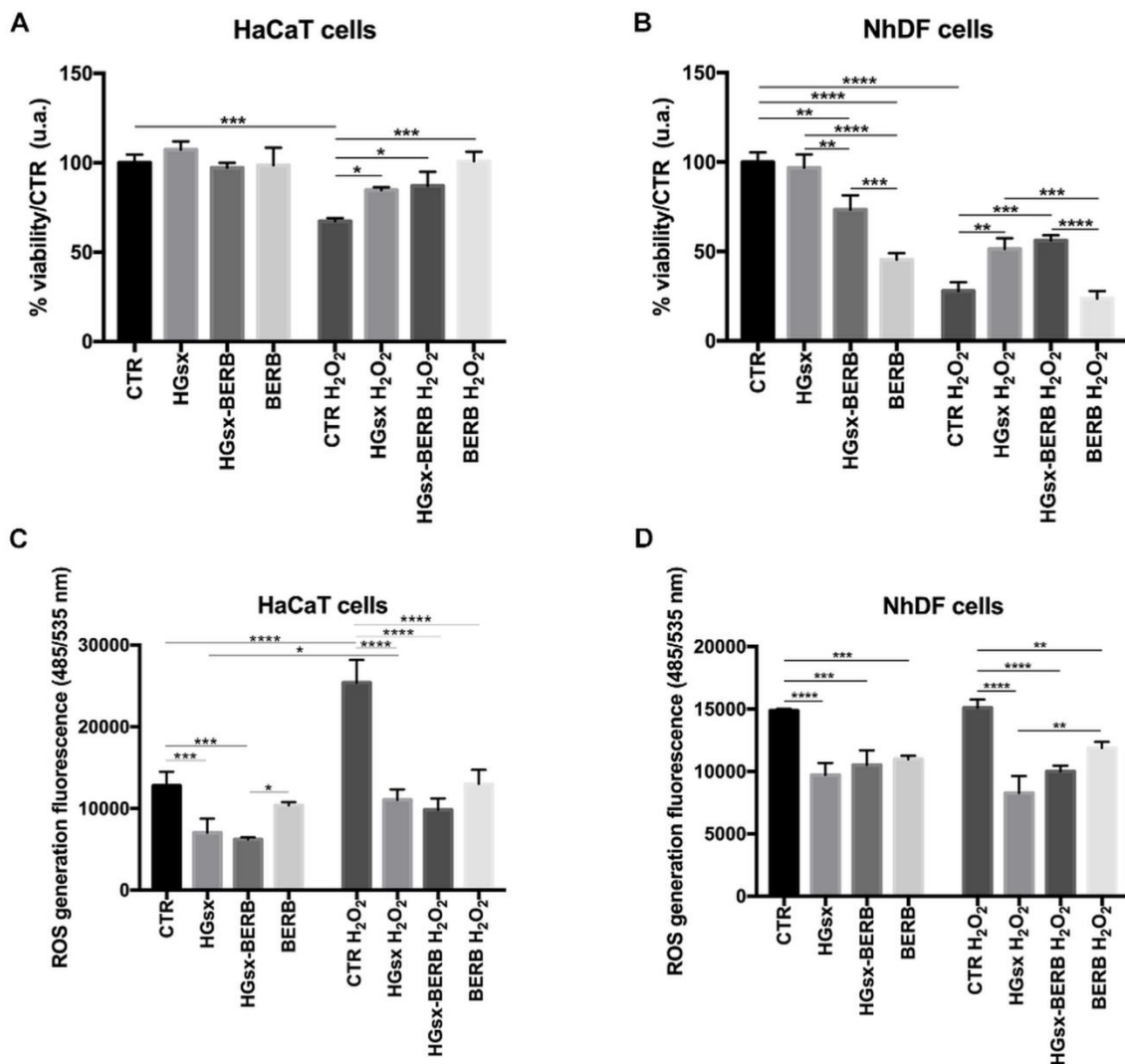
To investigate the effect of our systems on skin cells under normal and oxidative conditions, we evaluated viability on both HaCaT and NhDF at first.

Concerning HaCaT, cell viability at 48 h was not affected by HGsx, HGsx-BERB or BERB conditioned media and no significant differences were found among the groups. The oxidative condition caused the decrease of viability (59%) in control cells compared to the not-stressed ones, whilst the cells treated with HGsx, HGsx-BERB and BERB preserved good viability values, ranging between 75% and 89% (Fig. 4A). After 48 h, NhDF treated with HGsx-BERB and BERB showed a reduction in viability compared to the control and HGsx groups, even if the HGsx-BERB group maintained good viability (about 75%). Under oxidative stress conditions, not treated and BERB-treated fibroblasts underwent a significant reduction in viability (28% CTR; 24% BERB). Conversely, the cells conditioned with HGsx and HGsx-BERB showed better viability values than control ones, suggesting a tackle against oxidative damages (Fig. 4B).

Overall, these data confirm the antioxidant capacity of carboxymethyl cellulose (Fan L. et al., 2014) and suggest that the proposed association could be a useful tool for chronic wound management.

Whilst in acute wounds the levels of inflammatory cytokines, proteases, and reactive oxygen species (ROS) are low, in chronic wounds, the amounts of these molecules raise, with consequent increase of cell apoptosis and senescence, degradation of the tissue matrix, and impaired healing.

In particular, ROS are important for neutrophils and macrophages activities in acute wounds, but excessive ROS amount, as in chronic wounds, accelerates oxidative stress, inflammation and cellular damage (Morton et al., 2016; Wang et al., 2017; Cano Sanchez et al., 2018). Our results suggested that, in normal conditions, HGsx, HGsx-BERB and BERB did not affect HaCaT viability and have a limited effect on NhDF. The developed HGsx-BERB, taking advantage from its constituents, elicited a protective effect on both keratinocytes and fibroblasts subjected to H<sub>2</sub>O<sub>2</sub> stress, supporting cell viability.



**Fig. 4. Cell viability and ROS production in HaCaT and NhDF after 48 h.** Histograms representing viability percentage in HaCaT (A) and NhDF (B), with or without oxidative stress induction. Histograms showing ROS production in HaCaT (C) and NhDF (D), with or without oxidative stress induction. (\*  $p \leq 0.05$ ; \*\*  $p \leq 0.01$ ; \*\*\*  $p \leq 0.001$ ; \*\*\*\*  $p \leq 0.0001$ ).

### *3.2.2 ROS production*

In HaCaT, HGsx and HGsx-BERB conditioned media caused a slight, but significant, reduction in ROS production in normal conditions. After H<sub>2</sub>O<sub>2</sub> treatment, cells in the control group doubled their ROS expression. Cells of HGsx, HGsx-BERB, and BERB groups exhibited minor ROS amounts of 57%, 61% and 49% respectively, compared to control (Fig. 4C). We noted the same trend also in NhDF, where both HGsx and HGsx-BERB conditioned media were able to reduce ROS amounts comparing to the control group in both normal and oxidative environments (Fig. 4D).

In contrast to acute wounds, where the ROS levels are low and contribute to the beginning and support of injury healing, a prolonged inflammation phase causing impaired wound healing is partially connected to the presence of high ROS amounts (Cano Sanchez et al., 2018).

Our data showed that HGsx, HGsx-BERB and BERB treatments could be able to reduce ROS levels in both keratinocytes and fibroblasts, contributing to contrast tissue damage at the wound site caused by oxidative molecules. The control, but not the complete clearance, of ROS production in skin cells, could hinder the chronicity of the inflammatory stage and promote the prosecution of the wound healing process.

Once assessed the oxidative state of our cells, we went in-depth on the analysis of the effect of our materials only in stressed conditions.

### *3.2.3 Effect of HGsx, HGsx-BERB and BERB on oxidative stress markers*

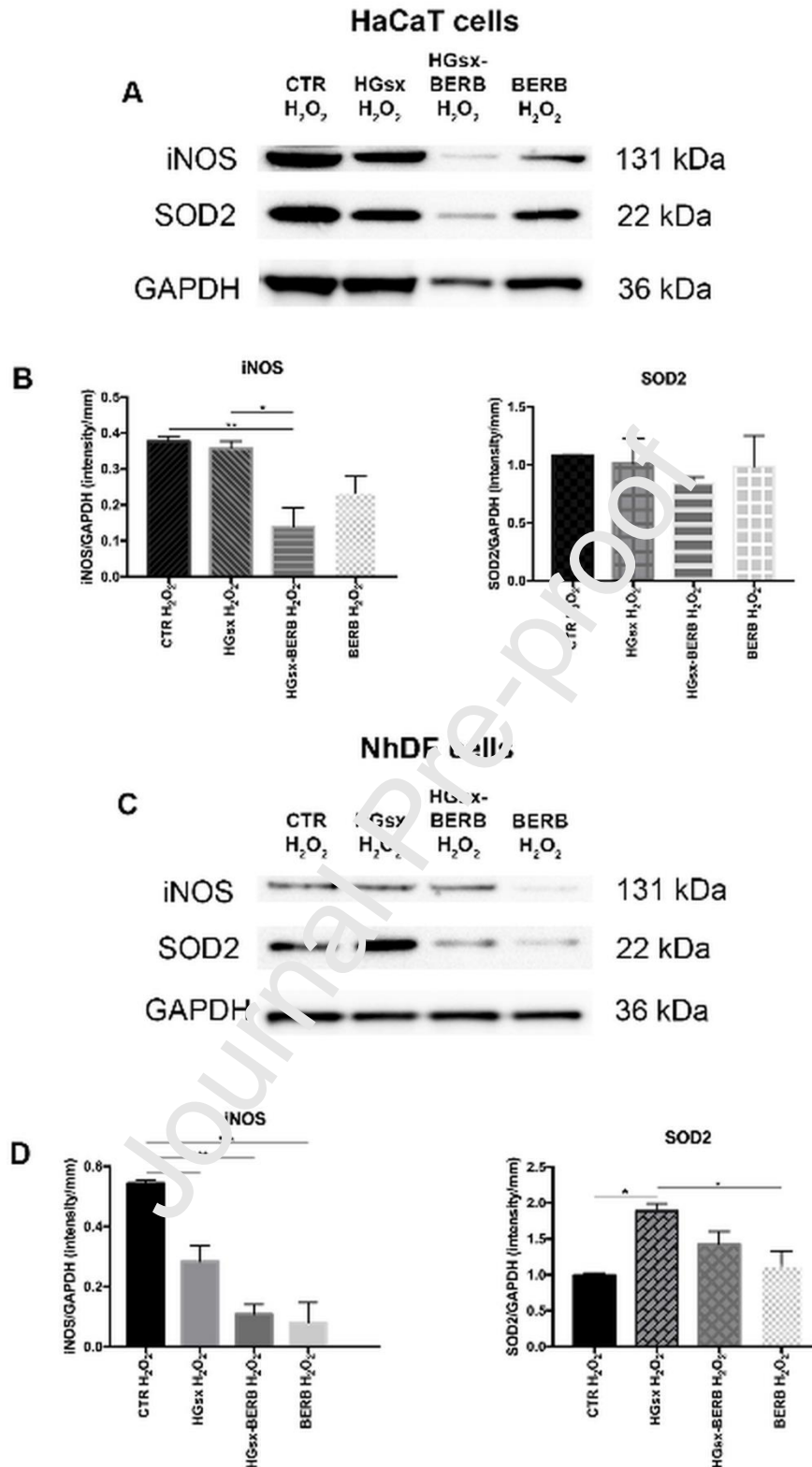
SOD2 is one of the major contributors as an antioxidant agent and promotes cell migration and proliferation in wound healing. It has been already shown that diminished SOD2 activity is correlated to diabetes, a disorder often associated with non-healing wounds (Bellot et al., 2019).

In HaCaT treated with HGsx-BERB, SOD2 levels were superimposable in all the groups (Fig. 5 A,B). Control NhDF showed lower SOD2 levels in oxidative conditions. Cells treated with HGsx and HGsx-BERB conditioned medium expressed higher SOD2 levels after oxidative stimulation, whilst the BERB group showed a small reduction in SOD2 amount (Fig. 5 C,D). Overall, we

observed that SOD2 levels were maintained high in both keratinocytes and fibroblasts treated with HGsx and HGsx-BERB after oxidative stress induction (Fig. 5). Therefore, the polymeric matrix of the film is as important as BERB, so their combination exploits the potential of both, sometimes highlighting how HGsx enhances BERB bioactive properties.

iNOS is an enzyme strictly related to acute inflammation: it produces Nitric Oxide (NO), which plays a central role in inflammatory and proliferative stages during wound healing (Wu et al., 2021). Excessive amounts of NO and iNOS have been detected in the wounds of diabetic patients, within the dermis, suggesting their involvement in inflammation chronicity and tissue damage (Wang et al., 2017; Saidian et al., 2019). Low iNOS expression was observed in HaCaT cells treated with HGsx-BERB and BERB. In control group, iNOS expression was 4-fold than in HGsx-BERB cells (Fig. 5 A,B). NhDF cells showed decreased iNOS expression in HGsx, HGsx-BERB and BERB treated cells compared to control (Fig. 5 C,D).

Taken together, these results suggested that HGsx and HGsx-BERB could be able to modulate the expression of proteins involved in oxidative stress response in skin cells. We suggest that HGsx and HGsx-BERB systems could stimulate the expression of anti-oxidative enzymes, while reducing the number of oxidative ones, thus contrasting chronicity in wounds.



**Fig. 5. Expression of oxidative stress markers in HaCaT and NhDF.** (A) Representative blots and (B) histograms for iNOS and SOD2 in HaCaT. (C) Representative blots and (D) histograms for iNOS and SOD2 in NhDF. (\*  $p < 0.05$ ; \*\*  $p < 0.01$ ).

### 3.3 Wound healing evaluation

#### 3.3.1 Co-localization and morphological evaluations

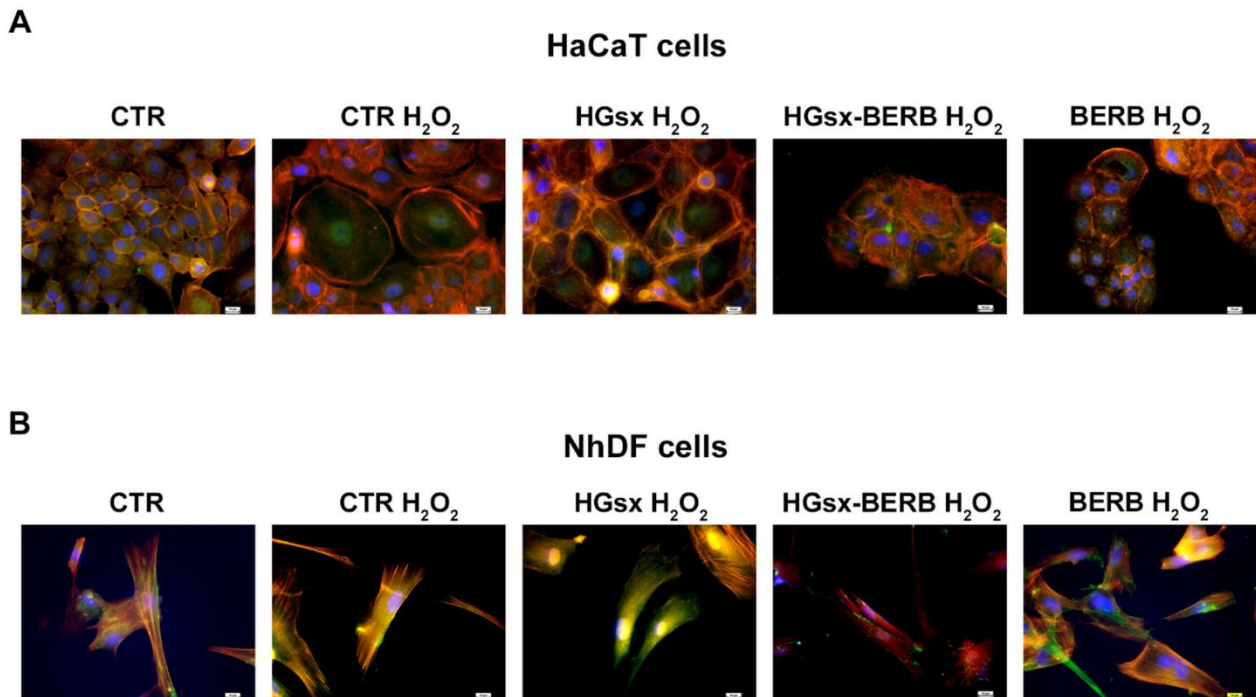
E-cadherin is a protein located in adherent junctions (AJs) between keratinocytes. Its interaction with the other AJ proteins and cytoskeletal actin allows the mechanical coupling of epithelial cells within the tissue, providing the potential for intercellular communication (Biswas et al., 2016).

E-cadherin/F-actin colocalization highlighted cell-cell junctions in untreated HaCaT cells, suggesting the integrity of the epithelial sheet. After oxidative stress, control cells exhibited an altered morphology with size increase, and a decrease of both E-cadherin and F-actin staining, suggesting a loss of intercellular junctions. Conversely, cells treated with HGsx and HGsx-BERB conditioned media presented stress fibres, normal morphology, and E-cadherin/F-actin colocalization were reestablished, suggesting the potential of these materials in the restoring of cell-cell junctions. In stressed cells treated with BERB, altered cell morphology and loss of E-cadherin/F-actin colocalization were still observed (Fig. 6A).

Fibronectin is a normal constituent of extracellular matrix (ECM) in the dermis and regulates cell-matrix interactions by membrane located integrins. This bond, involving also cytoskeletal actin to form the complex actin-integrin-fibronectin, influences cytoskeleton disposition and stress fibres assembly, affecting cell behavior and migration (Bloom et al., 1999). Fibronectin synthesis and deposition by fibroblasts are fundamental for ECM replacement and cell migration through the wound site (Liarte et al., 2020).

Unstressed cells showed spindle-shaped morphology, Fibronectin/F-actin colocalization in some parts, and the production of extracellular Fibronectin. After oxidative stress, a high grade of Fibronectin/F-actin colocalization, a decrease of extracellular staining, and an increase of intracellular stain for fibronectin were observed in fibroblasts of both control and HGsx groups. These alterations are comparable to those in the non-healing dermis. With HGsx-BERB treatment, NhDF cells restored their morphology, lost Fibronectin/F-actin colocalization, and highlighted a slight production of extracellular Fibronectin (Fig. 6B). This suggests that, in oxidative stress

conditions, HGsx-BERB treatment could stimulate fibroblasts to reestablish cell spindle-shaped morphology and the production of this extracellular matrix protein.



**Fig. 6. Double-labelling immunofluorescence on HaCaT and NhDF.** (A) Representative images of E-cadherin (green) and F-actin (red) staining and their co-localization (yellow) in HaCaT. (B) Representative images of Fibronectin (green) and F-actin (red) staining and their co-localization (yellow) in NhDF.

### 3.3.2 Expression of wound healing markers

To better define the role of HGsx and HGsx-BERB systems in wound healing, we evaluated in keratinocytes and/or fibroblasts the expression of proteins exerting different functions in the development/maintenance of wound chronicity.

NFkB p65 is a protein associated with inflammation, with a key role in the wound healing process (Liu et al., 2017). In the healing of an acute injury, during the inflammatory stage, NFkB p65 activation promotes the recovery, supporting cell proliferation and adhesion, and ROS clearance. In the subsequent healing phases, NFkB p65 is inactivated and its inhibition reduces keratinocytes proliferation, induces their differentiation, and promotes re-organization of junctions. In fibroblasts,

the deactivation of NFkB p65 reduces cell growth and migration. The impossibility to switch off the NFkB p65 activation extends the inflammation length, contributing to the wound chronicity (Liu et al., 2017; Wang et al., 2017; Cano Sanchez et al., 2018). HaCaT cultured with normal and HGsx-conditioned media presented higher NFkB p65 expression compared to HGsx-BERB treated cells, which exhibited the lowest protein levels, and BERB cells. (Fig. 7 A,B) In NhDF, the NFkB p65 amount decreased in all the treated groups, compared to the controls. (Fig. 7 C,D)

In wound healing, pro-inflammatory cytokines induce IDO1 expression in epithelial cells, and its levels increase at the wound site during the inflammatory stage: persisting high IDO1 concentrations after the inflammation phase delays wound healing (Ito et al., 2015). In HaCaT, IDO1 levels were visibly reduced (75%) after HGsx-BERB treatment, whilst its expression remained high in HGsx and BERB groups as in the control ones. (Fig. 7A,B)

After 2-10 days from injury, keratinocytes increase MMP9 expression, temporarily digesting ECM and migrating to the re-epithelialization site. In chronic wounds, high levels of MMP9 in keratinocytes damage the ECM, causing the production of inflammatory molecules that delay the healing process. MMP9 inhibition helps the injury restoration (Caley et al., 2015; Sabino et al., 2015; Lindley et al., 2016; Peng et al., 2021). In HaCaT after H<sub>2</sub>O<sub>2</sub> treatment, a substantial reduction of MMP9 protein was detected in HGsx and BERB cells and the expression was almost completely deleted in HGsx-BERB cells (Fig. 7 A,B).

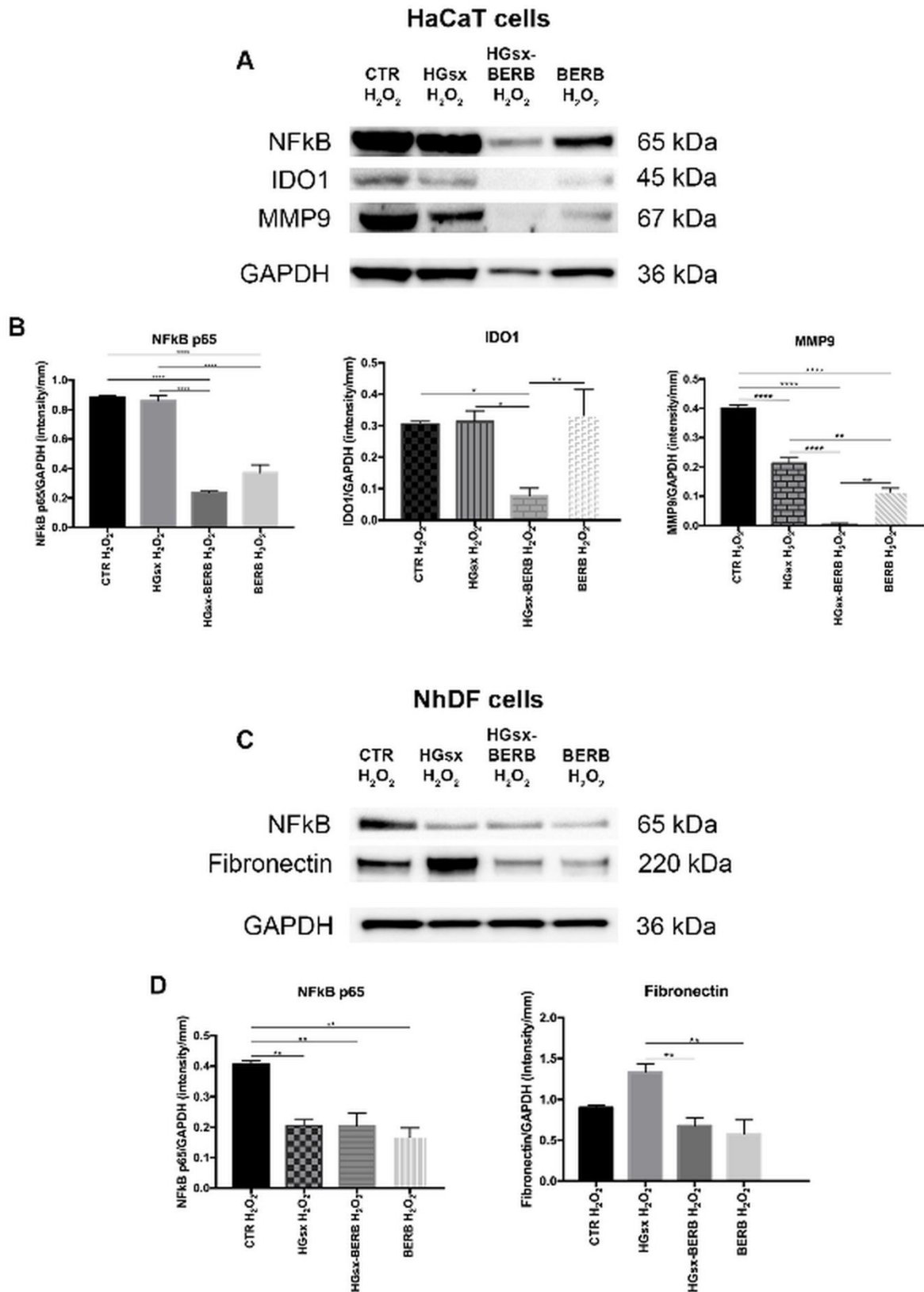
As stated before, in wound healing, Fibronectin is the main component of primitive ECM, and it is involved in cell-matrix interactions, fibrin clot stabilization, formation of granulation tissue, and cell migration. In chronic wounds, Fibronectin mRNA levels are significantly upregulated in the dermis. The concomitant excessive proteolytic Fibronectin degradation by several enzymes as metalloproteases (e.g., MMP9), causes an imbalance in ECM quality, with the presence of several Fibronectin fragments. (Liarte et al., 2020; Patten et al., 2021).

In the oxidant environment, we observe a high expression of Fibronectin in HGsx treated cells in comparison to the control culture. On the contrary, the Fibronectin levels in HGsx-BERB treated



cells were superimposable to controls, even if its amount was mainly extracellular as suggested by immunofluorescence observation. (Fig. 7 C,D)

Overall, HGsx-BERB treatment seems able to modulate the expression of several proteins fundamental in the self-renewing of the inflammatory stage in wound healing. Cells treated with this berberine-loaded hydrogel decreased NFkB and IDO1 expression in oxidative stress conditions, reducing the inflammatory contribution of these molecules to the non-healing mechanism. Moreover, under oxidative conditions, HGsx-BERB contrasted MMP9 expression in keratinocytes, thus preventing excessive ECM digestion and maintaining adequate Fibronectin extracellular levels in fibroblasts. This suggests that this hydrogel could act on both cell types supporting the healing process. Comparing HGsx-BERB to similar already studied berberine-loaded hydrogels (Zhang et al., 2020), we observed that our system was more effective in reducing NFkB and MMP9 expression, in comparison with the respective controls.



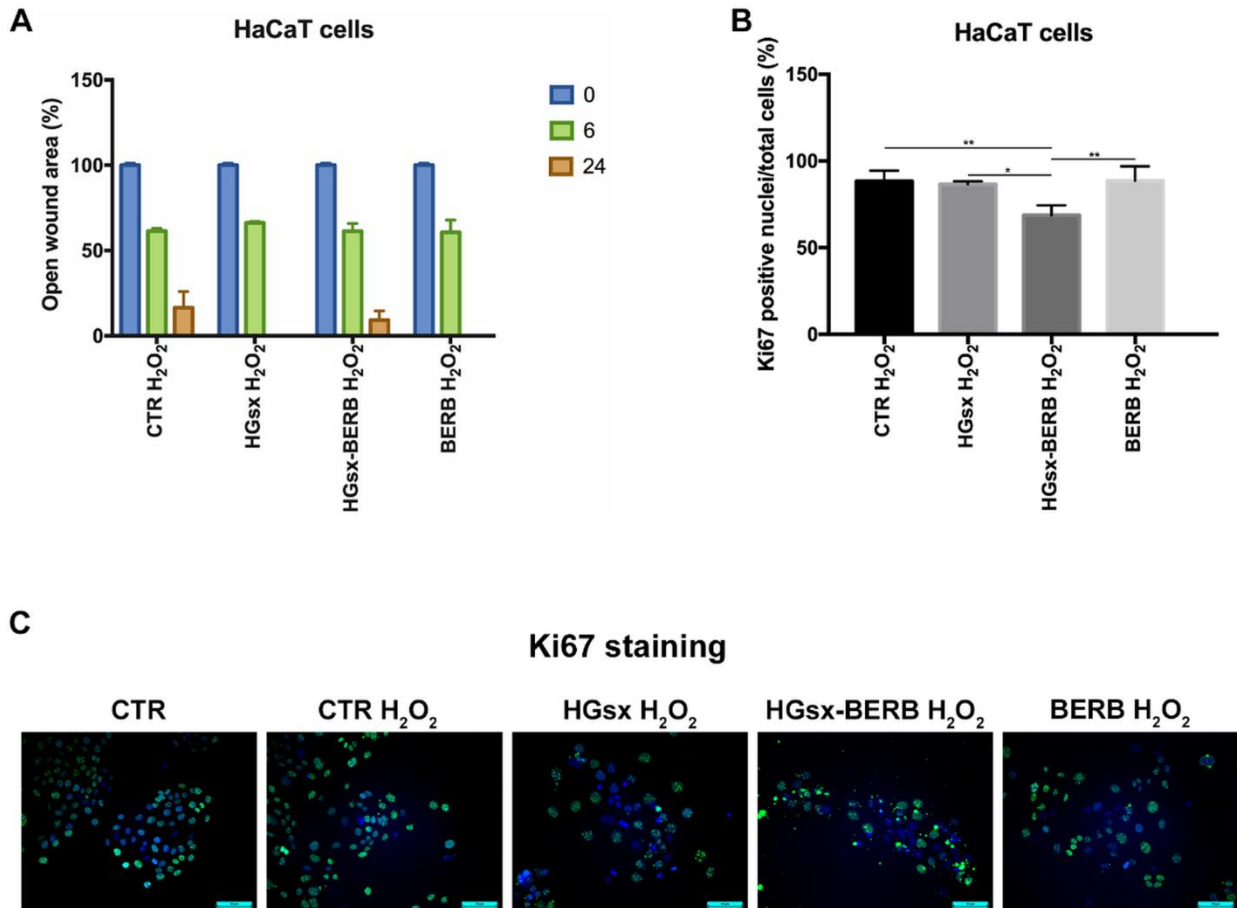
**Fig. 7. Expression of wound healing markers in HaCaT and NhDF.** (A) Representative blots and (B) histograms for NFkB p65, IDO1 and MMP9 expression in HaCaT. (C) Representative blots and (D) histograms for NFkB p65 and Fibronectin in NhDF. (\*  $p \leq 0.05$ ; \*\*  $p \leq 0.01$ ; \*\*\*  $p \leq 0.001$ ; \*\*\*\*  $p \leq 0.0001$ ).

On the other hand, our observations relevant to the HGsx activity are in agreement with Basu et al. (Basu et al., 2018) who applied CMC-based films in full-thickness wounds created in normal and diabetic rats. These Authors evidenced the capability of these films to faster the healing of both normal and diabetic (chronic) wounds. Moreover, the wound healing capability of hydrogels based on CMC and HEC, which are both components of our proposed system, as well as their anti-inflammatory activity have been also recently described in an *in vivo* experimental study (El Hosary et al., 2020).

### *3.4 Migration and proliferation in HaCaT cells*

Wound healing assay, performed to evaluate migratory capacity in stressed conditions, showed the presence of a similar gap among the groups at 6 hours from wound generation. At 24 hours from wound generation, untreated HaCaT showed wounds not completely closed, HGsx and BERB groups showed no gaps, whilst HGsx-BERB did not completely close the wound, although with no significant differences (Fig. 8A).

One of the side effects of wound healing is related to cell proliferation. In normal skin, or at the edge of acute wounds, proliferative keratinocytes are restricted at the basal layer, conversely in chronic wounds keratinocytes are mitotically active also in the upper layers. This results in parakeratosis and hyperkeratosis. Furthermore, the hyperproliferative epidermis fails to re-epithelialize and restore the skin barrier (Pastar et al., 2013). In this respect, we also evaluated the proliferative rate in HaCaT cells during stress conditions, highlighting that after H<sub>2</sub>O<sub>2</sub> treatment, HGsx-BERB conditioned cells showed a slight decrease in Ki67 expression (62%) compared to the other groups (Fig. 8 B,C).



**Fig. 8. HaCaT migration and proliferation.** (A) Percentage of wound area evaluation after 6 and 24 hours from the induced wound. (B) Histogram representing the percentage of Ki67 positive nuclei and (C) representative images of Ki67 staining (\*  $p < 0.05$ ; \*\*  $p < 0.01$ ).

HGsx-BERB did not affect migratory behavior in HaCaT with potential beneficial effects on keratinocytes towards re-epithelialization and is capable to control their proliferation in an oxidative environment, as in the case of chronic wounds.

### 3. Conclusions

In conclusion, HGsx and HGsx-BERB were characterized by different techniques evidencing the suitability of these biocomposites for wound healing applications. XPS and NMR evidenced the interaction between carbohydrate moieties and berberine. Moreover, our *in vitro* analysis provided a wide-ranging investigation of several aspects of chronic wound, such as chronic inflammation, permanent oxidative stress, tissue alterations and hyperkeratinization. Both developed systems display effects on viability preservation and ROS reduction, together with the modulation of

antioxidant and oxidative enzymes, on both keratinocytes and fibroblasts. Furthermore, after oxidative stress, HGsx-BERB treatment supported the restoration of morphology in HaCaT and NhDF cells, reestablishment of cell-cell junctions in keratinocytes and production of extracellular Fibronectin in fibroblasts. The moderate expression of inflammatory mediators (NFkB and IDO1), and degradative enzyme (MMP9) in HGsx-BERB treated cells, suggests the potential of this hydrogel in the escape from the chronic inflammatory loop. Moreover, we showed that HGsx-BERB could control keratinocytes proliferation without affecting migration, contrasting hyperkeratosis that preclude wound re-epithelialization.

Overall, the hypothesis that the addition of berberine to CMC-based hydrogel can enhance the material wound healing properties was confirmed. Indeed, this study demonstrated that this composite material is capable to control oxidative stress and inflammation in skin cells, and keratinocytes hyperproliferation, three typical hallmarks that prevent the injury restoration, suggesting its potential use for topical application in chronic wounds to promote the healing process.

## **Acknowledgements**

This work was carried out under the project “Study of new and completely biodegradable absorbent networks” financed by Italian Ministry of Economic Development (Dec. MISE F/050289/00/X32, September 15<sup>th</sup>, 2017, Horizon 2014-2020 PON I&C). Authors thank Eurofil s.r.l. (Castilenti, Teramo, Italy), in the person of Mr. G. Giannascoli. Professor Andrea Petrella (Politecnico of Bari, Italy) is greatly acknowledged for his precious collaboration in SEM measurements.

## **References**

Asadi, N., Pazoki-Toroudi, H., Del Bakhshayesh, A. R., Akbarzadeh, A., Davaran, S., & Annabi, N. (2020). Multifunctional hydrogels for wound healing: Special focus on biomacromolecular based hydrogels. *International Journal of Biological Macromolecules* 170, 728–750.

Bal- Öztürk, A., Özkahraman, B., Özbaş, Z., Yaşayan, G., Tamahkar, E., & Alarçin, E. (2021). Advancements and future directions in the antibacterial wound dressings—A review. *Journal of Biomedical Materials Research Part B: Applied Biomaterials*, 109(5), 703-716.

Basu, P., Narendrakumar, U., Arunachalam, R., Devi, S., Manjubala I. (2018) Characterization and Evaluation of Carboxymethyl Cellulose-Based Films for Healing of Full-Thickness Wounds in Normal and Diabetic Rats. *ACS Omega* 3, 12622–12632.

Bellot, G.L., Dong, X., Lahiri, A., Sebastin, S.J., Batinic-Haberle, I., Pervaiz, S., & Puhaindran, M. E. (2019). MnSOD is implicated in accelerated wound healing upon Negative Pressure Wound Therapy (NPWT): A case in point for MnSOD mimetics as adjuvants for wound management. *Redox Biology*, 20, 307–320.

Biswas, K.H., Hartman, K.L., Zaidel-Bar, R., & Groves, J.T. (2016). Sustained  $\alpha$ -catenin Activation at E-cadherin Junctions in the Absence of Mechanical Force. *Biophysical Journal*, 111(5), 1044–1052.

Bloom, L., Ingham, K.C., & Hynes, R.O. (1999). Fibronectin Regulates Assembly of Actin Filaments and Focal Contacts in Cultured Cells via the Heparin-binding Site in Repeat III13. *Molecular Biology of the Cell*, 10(5), 1521–1536.

Caley, M. P., Martins, V.L.C., & O’Toole, E.A. (2015). Metalloproteinases and Wound Healing. *Advances in Wound Care*, 4(4), 225–234.

Cano Sanchez, M., Lancel, S., Boulanger, E., & Nevriere, R. (2018). Targeting Oxidative Stress and Mitochondrial Dysfunction in the Treatment of Impaired Wound Healing: A Systematic Review. *Antioxidants*, 7(8), 98.

Capitani, D., Del Nobile, M.A., Mensitieri, G., Sannino, A., Segre, A.L. (2000) <sup>13</sup>C Solid-State NMR Determination of Cross-Linking Degree in Superabsorbing Cellulose-Based Networks *Macromolecules* 33, 430-437.

Capanema, N.S.V., Mansur, A.A.P., de Jesus, A.C., Carvalho, S.M., de Oliveira, L.C., Mansur, H.S. (2018) Superabsorbent crosslinked carboxymethyl cellulose-PEG hydrogels for potential wound dressing applications. *International Journal of Biological Macromolecules* 106, 1218–1234.

Cometa, S., Bonifacio, M. A., Licini, C., Bellissimo, A., Pinto, L., Baruzzi, F., Mattioli-Belmonte, M. & De Giglio, E. (2021). Innovative Eco-Friendly Hydrogel Film for Berberine Delivery in Skin Applications. *Molecules*, 26(16), 4901.

Condorelli, A. G., El Hachem, M., Zambruno, G., Nystrom, A., Candi, E., & Castiglia, D. (2021). Notch-ing up knowledge on molecular mechanisms of skin fibrosis: focus on the multifaceted Notch signalling pathway. *Journal of biomedical science*, 28(1), 1–17.

Fan, L., Peng, M., Zhou, X., Wu, H., Hu, J., Xie, W., Liu, S. (2014). Modification of carboxymethyl cellulose grafted with collagen peptide and its antioxidant activity. *Carbohydrate Polymers*, 112, 32-38.

Gao, J., Fan, D., Song, P., Zhang, S., & Liu, X. (2020). Preparation and application of pH-responsive composite hydrogel beads as potential delivery carrier candidates for controlled release of berberine hydrochloride. *Royal Society open science*, 7(11), 200676.

- Hebeish, A., Hashem, M., Abd El-Hady, M. M., & Sharaf, S. (2013). Development of CMC hydrogels loaded with silver nano-particles for medical applications. *Carbohydrate polymers*, 92(1), 407–413.
- Hosary, R.E.E., El-Mancy, S.M.S. El Deeb, K.S., Eid, H.H., EL Tantawy, M.E., Shams, M.M., Samir, R., Assar, N.H., Sleem, A.A. (2020) Efficient wound healing composite hydrogel using Egyptian *Avena sativa* L. polysaccharide containing  $\beta$  –glucan. *International Journal of Biological Macromolecules* 149, 1331 –1338.
- Hu, H., & Xu, F. J. (2020). Rational design and latest advances of polysaccharide-based hydrogels for wound healing. *Biomaterials science*, 8(8), 2084–2101.
- Huang, M.-J., Lee, K.S., Hurley, S.J. (2005) Nuclear magnetic resonance spectral analysis and molecular properties of berberine..*International Journal of Quantum Chemistry*, 105, 396–409,
- Ito, H., Ando, T., Ogiso, H., Arioka, Y., Saito, K., & Seishima, M. (2015). Inhibition of indoleamine 2,3-dioxygenase activity accelerates skin wound healing. *Biomaterials*, 53, 221–228.
- Jiang, D., & Rinkevich, Y. (2021). Distinct fibroblasts in scars and regeneration. *Current Opinion in Genetics & Development*, 70, 7-14.
- Kanikireddy V., Varaprasad K., Jayaramuduc T., Karthikeyan C., Sadiku R. (2020). Carboxymethyl cellulose-based materials for infection control and wound healing: A review. *International Journal of Biological Macromolecules* 164, 963-975.
- Kumar, B., Deeba, F., Priyadarshi, R., Bano, S., Kumar, A., & Negi, Y. S. (2020). Development of novel cross-linked carboxymethyl cellulose/poly (potassium 1-hydroxy acrylate): Synthesis, characterization and properties. *Polymer Bulletin*, 77(9), 4555–4570.



- Liarte, S., Bernabé-García, Á., & Nicolás, F.J. (2020). Role of TGF- $\beta$  in Skin Chronic Wounds: A Keratinocyte Perspective. *Cells*, 9(2), 306.
- Lin, X., Li, Y., Chen, Z., Zhang, C., Luo, X., Du, X., & Huang, Y. (2013). Synthesis, characterization and electrospinning of new thermoplastic carboxymethyl cellulose (TCMC). *Chemical engineering journal*, 215, 709-720.
- Lindley, L.E., Stojadinovic, O., Pastar, I., & Tomic-Canic, M. (2016). Biology and Biomarkers for Wound Healing. *Plastic and Reconstructive Surgery*, 138(3S), 18S.
- Liu, T., Zhang, L., Joo, D., & Sun, S.C. (2017). NF- $\kappa$ B signaling in inflammation. *Signal Transduction and Targeted Therapy*, 2(1), 1–9.
- Morton, L. M., & Phillips, T. J. (2016). Wound healing and treating wounds: Differential diagnosis and evaluation of chronic wounds. *Journal of the American Academy of Dermatology*, 74(4), 589–605.
- Oun, A. A., & Rhim, J. W. (2015). Preparation and characterization of sodium carboxymethyl cellulose/cotton linter cellulose nanofibril composite films. *Carbohydrate Polymers*, 127, 101–109.
- Pastar, I., Stojadinovic, O., Yin, N.C., Ramirez, H., Nusbaum, A.G., Sawaya, A., Patel, S.B., Khalid, L., Isseroff, R.R., & Tomic-Canic, M. (2014). Epithelialization in Wound Healing: A Comprehensive Review. *Advances in Wound Care*, 3(7), 445–464. <https://doi.org/10.1089/wound.2013.0473>
- Patten, J., & Wang, K. (2021). Fibronectin in development and wound healing. *Advanced Drug Delivery Reviews*, 170, 353–368.
- Peng, Z., Nguyen, T.T., Song, W., Anderson, B., Wolter, W.R., Schroeder, V.A., Hesk, D., Lee, M., Mobashery, S., & Chang, M. (2021). Selective MMP-9 Inhibitor (R)-ND-336 Alone or in

Combination with Linezolid Accelerates Wound Healing in Infected Diabetic Mice. *ACS Pharmacology & Translational Science*, 4(1), 107–117.

Sabino, F., & auf dem Keller, U. (2015). Matrix metalloproteinases in impaired wound healing. *Metalloproteinases In Medicine*, 2, 1–8.

Saidian, M., Lakey, J.R.T., Ponticorvo, A., Rowland, R., Baldado, M., Williams, J., Pronda, M., Alexander, M., Flores, A., Shiri, L., Zhang, S., Choi, B., Kohen, R., Tromberg, B.J., & Durkin, A.J. (2019). Characterisation of impaired wound healing in a preclinical model of induced diabetes using wide-field imaging and conventional immunohistochemistry assays. *International Wound Journal*, 16(1), 144–152.

Schindelin, J., Arganda-Carreras, I., Frise, E., Kaynig, V., Longair, M., Pietzsch, T., Preibisch, S., Rueden, C., Saalfeld, S., Schmid, B., Tinevez, J., White, D.J., Hartenstein, V., Eliceiri, K., Tomancak, P., & Cardona, A. (2012). Fiji: an open-source platform for biological-image analysis. *Nature methods*, 9(7), 676–682.

Stan, D., Tanase, C., Avram, M., Apetrei, R., Mincu, N. B., Mateescu, A. L., & Stan, D. (2021). Wound healing applications of creams and “smart” hydrogels. *Experimental Dermatology*, 1–15.

Tejiram, S., Kavalukas, S.L., Shupp, J.W., & Barbul, A. (2016). 1—Wound healing. In M. S. Ågren (Ed.), *Wound Healing Biomaterials*, 3–39. Woodhead Publishing.

Trapani A., De Giglio E., Cafagna D., Denora N., Agrimi G., Cassano T., Gaetani S., Cuomo V., Trapani G. (2011). Characterization and evaluation of chitosan nanoparticles for dopamine brain delivery. *International Journal of Pharmaceutics*, 419, 296–307.

Wang, T., He, R., Zhao, J., Mei, J.C., Shao, M.Z., Pan, Y., Zhang, J., Wu, H.S., Yu, M., Yan, W.C., Liu, L.M., Liu, F., & Jia, W.P. (2017). Negative pressure wound therapy inhibits inflammation and

upregulates activating transcription factor-3 and downregulates nuclear factor- $\kappa$ B in diabetic patients with foot ulcerations. *Diabetes/Metabolism Research and Reviews*, 33(4), e2871.

Wu, M., Lu, Z., Wu, K., Nam, C., Zhang, L., & Guo, J. (2021). Recent advances in the development of nitric oxide-releasing biomaterials and their application potentials in chronic wound healing. *Journal of Materials Chemistry B*, 9(35), 7063–7075.

Zhao, R., Liang, H., Clarke, E., Jackson, C., & Xue, M. (2016). Inflammation in Chronic Wounds. *International Journal of Molecular Sciences*, 17(12), 2085.

Zhang, P., He, L., Zhang, J., Mei, X., Zhang, Y., Tian, H., & Chen, Z. (2020). Preparation of novel berberine nano-colloids for improving wound healing of diabetic rats by acting Sirt1/NF- $\kappa$ B pathway. *Colloids and Surfaces B: Biointerfaces*, 187, 110647.

Zhang, M., Yang, M., Woo M.W., Li, Y., Han, W., Dang, X.(2021) High-mechanical strength carboxymethyl chitosan-based hydrogel film for antibacterial wound dressing *Carbohydrate Polymers*,256 117590.

Zhang, K., Wang, Y., Wei, Q., Li, X., Guo, Y., Zhang, S. (2021) Design and Fabrication of Sodium Alginate/Carboxymethyl Cellulose Sodium Blend Hydrogel for Artificial Skin. *Gel* 7, 115.

Zohuriaan-Mehr, M., Kabiri, K. (2008) Superabsorbent Polymer Materials: A Review. *Iranian Polymer Journal* 17(6), 451-477.

## **Credit Authors Statement**

Conceptualization, Cometa S., Mattioli-Belmonte M., De Giglio E.; Methodology, Cometa S., Licini C., Bonifacio M.A., Mastrorilli P.; Investigation, Cometa S., Licini C., Bonifacio M.A., Mastrorilli P.; Data curation, Cometa S., Licini C., Bonifacio M.A., Mastrorilli P.; Writing original draft preparation, all authors; Writing—review and editing, all authors; Supervision, De Giglio E.; Funding acquisition, Cometa S., Mattioli-Belmonte M., De Giglio E..

All authors have read and agreed to the published version of the manuscript.

**Declaration of interests**

The authors declare that they have no known competing financial interests or personal relationships that could have appeared to influence the work reported in this paper.

Graphical abstract

